Roles of Vanadium and Nitrogen in Photocatalytic Activity of V-N-codoped TiO_2 Photocatalyst

Ranjana Varma[1*], ManishaYadav[2], Kajal Tiwari[1], Nisha Makani[1], S. Gupta[1]

D. C. Kothari[1], A. Miotello[3], N. Patel[1, 2#],

[1]Department of Physics, University of Mumbai, Santacruz (E), Mumbai 400 098, India

[2]National Centre for Nanosciences& Nanotechnology, University of Mumbai, Santacruz (E), Mumbai 400 098, India

[3]Dipartimento di Fisica, UniversitàdegliStudi di Trento, I-38123 Povo, Trento, Italy

Correspondingauthors e-mail address:[*]ranju16@gmail.com,[#]nainesh11@gmail.com.

Abstract

Recent advancement of multi elements codoped-TiO_2 in photocatalytic application demands to understand the role of each dopant involved in catalytic mechanism. Here we explore the VN-codoped TiO_2 system intended to understand the role played by each dopant in synergistic enhancement in performance of TiO_2 semiconductor. The concentrations of V and N were varied and optimized to improve photocatalytic activity. The photocatalytic decomposition of phenol and dye in aqueous solution under visible light was used as a probe reaction to evaluate their performance. With increase in vanadium concentration in VN-codoped TiO_2 considerable improvement in visible light absorption is observed as compared to nitrogen doping due to the effective narrowing of the band gap from 3.12 eV to 1.88 eV. At low concentration, the energy levels formed by both V and N act as the trapping centers for photo-generated charges to suppress recombination process as indicated by PL and TRPL results. As V concentration increases, recombination centers are created in form of oxygen vacancies as confirmed by XPS. Addition of N partially fills these oxygen vacancies to reduce the amount of recombination and prolong the lifetime of charge carriers.V improves the visible light absorption to generate large number of electron-hole pair while N reduces the recombination of electron-hole pair creating the synergetic effect to produce three times better performance than pure TiO_2.

Keywords: Photocatalyst, Codoped TiO_2, visible light absorption, Organic pollutant degradation,

1. Introduction

TiO_2 is an extensively investigated semiconductor for photocatalytic applications because of its easy availability, environment friendliness, low-cost, stability, photo-corrosion resistance in aqueous media and appropriate band-edges [1, 2]. However, poor visible light absorption owing to its bandgap of 3.2 eV and high recombination rates of photo-generated charge carriers leads to low photocatalytic efficiency of TiO_2. For its widespread usage, it is necessary to solve both these problems to achieve high photocatalytic activity under solar light. Scientists in the past have focused on modifying TiO_2 by doping foreign elements to reduce the band gap and/or to increase the lifetimes of the charge carriers [3]. Metallic dopants such as V, Cu, W, Cr and non-metallic dopants such as N, C, S are known to modify the bandgap by forming energy levels near to conduction band and valance band, respectively [4-9]. Thus, these dopant levels effectively reduce the band-gap of TiO_2 causing red shift in the absorption band and consequently increasing the visible light absorption. At certain optimum concentration, impurity energy level introduced within the band gap also act as the trapping site to reduce recombination process, while above this concentration the level act as the recombination sites. This optimization normally exists at very small doping concentration where the band gap narrowing is minimal. Along with it the single impurity can trap only one type of charge carrier either e^- or h^+.

Codoping TiO_2 with metal and non-metal elements, with optimized concentrations, creates energy levels at both the ends of bands to effectively reduce the forbidden gap [10-12]. Energy levels introduced by codoping can trap both the e^- and h^+ individually to reduce recombination process. In addition, hybridization between dopants creates extra states within the band gap to facilitates both light absorption and charge separation. Due to the synergistic effect, Vanadium-Nitrogen (V-N) codoping in TiO_2 have gained particular attention for their ability to successfully

enhance several photocatalytic reactions. The VN-codoping pair allows the decrease of the band gap and the passivation condition. In addition, the calculated band edges match the redox potentials of hydroxyl radical and superoxide anion [13]. There are various studies reported in the literature on the photocatalytic activity of vanadium and nitrogen codoped-TiO_2 [6,8,14-16]. The extensive work carried out by our group indicated various factors contributing the enhancement in photocatalytic efficiency of VN-codoped TiO_2 under visible light irradiation [6]. Some of these factors are: specific surface area of TiO_2 nanoparticles, band gap narrowing, traps states produced by the dopants, and separation of charges. While the VN-codoped TiO_2 is a promising photoactive material in chemical reactions, understanding the role of each dopant in the photoresponse mechanisms is rather limited. Collectively both V and N assist in considerable band gap reduction, charge trapping and separation, charge transport to surface, formation of oxygen vacancies, absorption of reactants and OH- group on surface, and improvement in surface area. However, which of these mechanisms are dominant in VN-codoped TiO2 and what are the roles of V and N in influencing the pathways are not yet studied.

The present study was designed to isolate each factors affecting the photo-activity and focus on the role played by each dopant (V and N) under visible light irradiation by varying concentration of V and N in V-N-codoped TiO_2. The recombination rates and lifetimes of the charge carriers in the pure and doped TiO_2 nanoparticles were examined using steady state Photoluminescence (PL) and Time Resolved Photoluminescence (TRPL) spectroscopy techniques. The photocatalytic properties of the VN-codoped TiO_2 were determined by monitoring the degradation of p-nitrophenol (PNP) and methyleneblue (MB). The relation between of the observed photocatalytic activity of VN-codoped TiO_2 samples with their band gap values and lifetimes for the corresponding samples was established.

2. Experimental

A series of VN-codoped TiO_2 photocatalysts with different vanadium and nitrogen dopant concentrations were prepared by sol gel method as described in previous work [6]. In a typical procedure, titanium (IV) butoxide ($Ti(OC_4H_6)$), tri-ethylamine ($N(CH_2CH_3)_3$) and ethanol were mixed together and stirred for 1 h. In parallel, sodium metavanadate (NH_4VO_3) was dissolved in water with addition of HNO_3 to maintain the pH of the mixture at about 1.2. The VN-codoped TiO_2 was produced by mixing the above two solutions under vigorous stirring for 4 h at ambient temperature. For gelation resulting solution was kept overnight before washing two times with ethanol and one time with water followed by drying at 120 ^oC for 2 h to remove the excess solvent. The resultant powder material was then annealed at 450 ^oC for 2 h in air to prepare the final VN-codoped TiO_2 samples. The undoped TiO_2 was prepared by the same approach without the addition of vanadium and nitrogen precursors. The sample nomenclature used in the present work is shown in **Table 1**. For cooping, two approaches are used; in the first case the concentration of V was maintained constant (2 at %) and concentration of nitrogen was varied in the range of 1- 4 at. %. This concentration, labelled as 2VxN, was selected because the photocatalytic activity of V-doped catalysts was maximum at 2 at% [6]. In the second approach the concentration of N was maintained constant (4 at %) while varying concentration of V was varied between 1 to 4 at.%. the choice was driven by the fact that the photocatalytic activity of N-doped catalysts was maximum at 4 at% [6, 16].

The phase composition of the as-prepared samples was determined by a Rigaku Ultima IV X-ray diffraction (XRD) pattern with Cu K_α radiation (40 kV and 40 mA). The surface composition and chemical states of the samples were examined by X-ray photoelectron spectroscopy (XPS) using an AXIS Supra (Kratos Analytical) instrument equipped with a

monochromatic Al K_α (1486.6 eV) X-ray source. All the binding energy (BE) positions were referenced to C 1s (284.8 eV) peak. The UV-Vis diffuse reflectance spectra (DRS) of the samples were recorded on a Cary 500 UV-Vis spectrophotometer with an integrating sphere assembly. $BaSO_4$ was used as a reflectance standard in the wavelength range of 200∼800nm. Fourier transform infrared spectra (FT-IR) were recorded in a Perkin Elmer, Frontier equipment using KBr pellet method. Brunauer–Emmett–Teller (BET) specific surface area measurements were carried out by determining the N_2 adsorptionand desorption isotherms on a single point BET surfacearea system (Smart SORB 93) after degassing the entire samples at 120 ^oC for 2 h. Transmission Electron Microscope (TEM) and Energy-dispersive X-ray spectroscopy (EDS) mapping were taken with FEG-TEM 200 kV (JEM-2100F). The steady state photoluminescence (PL) studies were carried out using a fluorescence spectrophotometer (Varian; Cary Eclipse) at two excitation wavelengths (280 nm and 385 nm). Time resolved photoluminescence (TRPL) studies were carried out using the ISS Chronos BH model equipped with a picosecond pulsed (70ps) laser diode from Hamamatsu with a wavelength of 405 nmand a peak power of 100 mW. Glycogen dispersed in distilled water was used as a scattering sample to measure the instrument response function (IRF). To acquire PL spectra, 3 mg of powder photocatalyst was dispersed in 10 ml of DDW and transferred into a 1 cm × 1 cm quartz cuvette for measurement.

Photocatalytic activity test

The photocatalytic activity of the as synthesized catalysts was evaluated by photocatalytic decomposition of para-nitrophenol (PNP) and methylene blue (MB) solutions. The experiments were carried out in a 250 mL of photochemical glass reactor and a 150 W xenon lamp (Hamamatsu) as a visible-light source placed at about 47 cm from the photoreactor. In each run, 20 mg photocatalyst was added into 50 mL PNP or MB solution of 10 mgL^{-1}. Prior to irradiation,

the suspension was kept in the dark under stirring for 20 min to ensure the establishing of an adsorption/desorption equilibrium. After visible-light irradiation for 20 min, 3 mL of reaction solution was withdrawn to check the pollutant concentration. The concentration of organic pollutant left in the aqueous system was monitored by detecting the intensity of absorption peak at wavelength at 320 nm and 665 nm for PNP or MB respectively. UV-Vis absorption spectra were recorded on a UV-Vis spectrophotometer (Implen Nano Photometer™ Pearl). After measurement, the sample was put back to the reaction solution to conduct the photo-degradation experiments with the same procedure as mentioned above. A blank test was also carried out by irradiating the pollutant (PNP or MB) solution without photocatalyst. All the experiments were repeated three times to verify the consistency. The photocatalytic activity was quantified using the photodegradation rate efficiency determined from the pseudo first order law and also the percentage degradation (%) has been evaluated [17].

3. Results and discussion

Fig. 1 (a-b) shows the X-ray diffraction patterns of 2VxN and xV4N-codoped TiO_2 samples including data for undoped TiO_2, used here as a reference. Except phases related to TiO_2 no other diffraction peaks are observed in the codoped samples. No characteristic peak of vanadium oxide was found in the XRD patterns implying either that vanadium was incorporated in the lattice structure of TiO_2 or that vanadium oxide amount was very small and highly dispersed. All the as-prepared TiO_2 materials show single TiO_2 anatase phase except for 2V0N and 4V4N sample, which contain small amount of rutile phase as well. In case of V-doped TiO_2 (2V0N), presence of metal dopant such as V creates oxygen vacancies in the TiO_2 lattice which lead to the

breakage of Ti-O bonds in anatase structure to form rutile phase. However, in VN-codoped TiO_2 inclusion of N fills these oxygen vacancies to inhibit the anatase to rutile conversion. At highest concentration of V doping (4V4N), the amount of nitrogen might be not enough to fill all the O vacancies thus forming small amount of rutile phase. Nevertheless this shows that V and N substitutionally replace Titanium and Oxygen in TiO_2 lattice to disrupt the crystal structure (also confirmed by XPS in next section). **Table 1** lists the crystal size of all codoped TiO_2 samples which were calculated by Scherrer equation. The observed particle size is of the order of 10 nm. No lattice distortion was observed because the ionic radius of V^{4+} (0. 72 A) is very close to that of Ti^{4+} in TiO_2 (0.74 A) and so V^{4+} ions easily substitute Ti^{4+} ions in TiO_2 lattice.

The presence of oxygen vacancies was confirmed using XPS technique conducted on four samples (pure TiO_2, 2V, 2V4N and 4V4N TiO_2) and shown in **Fig. 2**. In Ti 2p core level, two peaks centred at 458.7 eV and 464.6 eV attributed to Ti $2p_{3/2}$ and Ti $2p_{1/2}$ of Ti^{4+} state in TiO_2 are observed for pure TiO_2 [18]. After addition of 2V and 2V4N, these peaks appear broad with a shoulder at lower binding energy. Deconvolution of peaks at Ti $2p_{3/2}$ shows the existence of two peaks assigned to Ti^{4+} (458.6 eV) in anatase TiO_2 and Ti^{3+} (456.6 eV) formed due to oxygen vacancy [6]. In case of highest level of doping (4V4N) both these peaks are distinctly separated with marginal shift of 0.3 eV of Ti^{4+} peak (459 eV) as compared to undoped TiO_2. This suggests that the V and N are incorporated into TiO_2 lattice, in agreement with XRD results, to influence the local chemical state of Ti^{4+} ions. The ratio of Ti^{3+}/Ti^{4+} is highest for 4V4N TiO_2 while for 2V-doped TiO_2 the ratio decreases by small amount after inclusion of 4N in 2V4N sample. In 2V4N TiO_2 sample, the V $2p_{3/2}$ level was deconvoluted into two peaks with BE centered at 516.5 eV and 514.3 eV. Former peak arises due to V^{4+} species formed by replacing Ti^{4+} substitutionally in TiO_2 matrix. The peak at lower BE is assigned to vanadium in V-N bonds [NIST XPS database] thus

suggesting the hybridization between V and N dopants. The peak in N 1s level was also deconvoluted into two peaks, where major peak at 399.5 eV is contributed by N substitutionally replacing O to form O-Ti-N linkage. The small peak at 397.2 eV is attributed to V-N bond thus confirming the interaction between dopants [NIST XPS database]. For other two samples (2V-TiO_2 and 4V4N-TiO_2), the V and N are present in similar chemical state with little more amount of V-N bonds in case of 4V4N-codoped TiO_2 (figure not shown). This result indicates that V substitutionally replaces the Ti in the lattice leading to the formation of oxygen vacancy whose number increases with V concentration. Later, these oxygen vacancies are partially filled by addition of N. However, for 4V4N the amount of nitrogen is not enough to fill the majority of oxygen vacancies, as indicated by XRD result, thus forming mixed anatase and rutile phases. Substitutional replacement of Ti and O with V and N, respectively, leads to hybridization between V and N to form V-N bonds. The atomic concentration of Ti, O, V and N on the surface was evaluated as 27.8 %, 67.2 %, 3.33 % and 1.68 % respectively. The higher oxygen content is owing to the hydroxyl group attached to the surface as confirmed by FTIR in next section.

The Fourier transform infrared spectroscopy (FTIR) spectra of samples are shown in **Fig. 3**. All the samples show a band in the region of 400-800 cm^{-1} attributed to Ti-O stretching and Ti-O-Ti bridging stretching modes,and O-Ti-O bending vibrations of anatase TiO_2 [19, 20]. With the increase of vanadium concentration a broad band is observed in the region 3000−3600 cm^{-1} ascribed to stretching vibration of surface hydroxyl groups and absorbed water molecules. This result specifies that V ions result beneficial for the hydroxyl groups and attract more hydroxyl groups on the surface of the TiO_2 samples: this might aid in the degradation of the dye on the surface of the catalyst. The small bands around 844 and 580 cm^{-1} are the signature peak for the stretching vibration of O=V=O in vanadium oxide [21].

UV-Vis absorption spectra of pure and doped TiO_2 are displayed in **Fig. 4 (a, b)**. As compared to pure TiO_2, the optical band edge is red shifted for all the doped and codoped TiO_2 irrespective of type and concentration of dopants. The energy band gap values obtained by using Tauc plot (Fig. S1) are summarized in **Table 1**. The value of 3.12 eV measured for bare TiO_2 is very close to that reported for anatase phase of TiO_2 (3.2 eV). By doping with nitrogen, the band gap value is marginally decreased to a value of 3.05 eV while noticeable narrowing in band gap is observed by V doping, up to 2.42 eV for 2V0N. Combining both V and N creates significant reduction in band gap with minimum value of 1.88 eV recorded for highest doping concentration (4V4N). For codoped xV4N samples the band gap value decreases with increase in V concentration while for 2VxN the narrowing is nearly same for all the concentration of N. This suggests that V doping is predominately effective in making TiO_2 more active in visible light range. The theoretical DFT calculation conducted in our past work on VN-codopedTiO_2 [8] indicates that N 2p states are formed above the valance bands maxima (VBM) which merges with VB of TiO_2 to reduce the band gap by small amount as in case of 0V4N. For V doped TiO_2, isolated charge states of V 3d orbitals are formed at 0.7-0.9 eV below the conduction band minima (CBM). In addition to the presence of these isolated bands, hybridization between V-N electronic orbitals creates a further narrowing of band gap by the overlapping of density of states (DOS) near VBM. This theoretical band gap model is in good agreement with experimentally obtained results for the present TiO_2, 2V doped, 4N doped and 2V4N-codoped TiO_2. XPS spectra demonstrates that V and N substitutionally replaces Ti and O to induce isolated localized level within the band gap. In addition to these impurity levels, the hybridization between V-N, also confirm by XPS causes further narrowing in band gap of V-N-codoped TiO_2. In xV4N, the increase in V concentration creates the oxygen vacancies, as confirmed by XPS and XRD results, which are known to form

deep levels at 1.0-1.2 eV below the CBM in band gap [22, 23]. Indeed, this oxygen vacancy is responsible for reduction of band gap in addition to the isolated V^{4+} based impurities state and being more efficient with increasing concentration of V in codoped TiO_2. On the other hand, the effect of oxygen vacancies is partially nullified due to increase in nitrogen concentration for 2VxN to maintain the band gap nearly constant with N concentration.

The 2V4N showed the highest photo catalytic activity, so TEM of this sample was performed and presented in **Fig. 5 (a)**. TEM micrograph of 2V4N sample shows (**Fig. 5 (a)**) that most of the particles are of spherical shape. The average particle size of 2V4N-codoped TiO_2 nanoparticle is found to be about 10 ± 2 nm which is in good agreement with crystal size obtained with XRD. The nano-scale size of particle offers greater surface area to volume ratios and thus induces better surface absorbability of hydroxyl/water, which in-turn acts as an active oxidizer in the photocatalytic reaction. The presence of lattice fringes was clearly visible in HRTEM image **(Fig. 5 (b))** of an individual particle hence suggesting the crystalline nature of the photocatalyst particle. Interplanar spacing of 0.354 nm was measured between the lattice fringes in HETEM image. This value matches well with the spacing value of the anatase phase (0.352 nm) of {1 0 1} family of planes. The EDX pattern of the codoped sample (**Fig. 6)** shows the presence of Ti, O, V and N as a constituent in the prepared doped nanoparticle. For 2V4N-codoped TiO_2 nanoparticles the amount of Ti, O, V and N in at % is found to be 25.70%, 68.35% and 1.98 % and 3.97 % respectively. Elemental mapping images (**Fig. 6**) indicates uniform distribution of V and N atoms in the TiO_2 thus suggesting the successful formation of VN-codoped TiO_2. The BET surface areas of all the samples are listed in **Table 1**. Though no major variation in the surface area is observed among the samples; large BET specific surface area of every sample indicates relatively high surface-to-volume ratio achieved with smaller particle size (~ 10 nm).

Fig. 7 (a-b) shows the room temperature PL spectra of samples, taken with an excitation wavelength of 280 nm. The broad band centred at 385 nm with the presence of shoulder at 400-425 nm along with strong emission peak in the NIR region at 845 nm are observed for all the samples. The broad emission peak at about 385 nm wavelength is ascribed to the emission due to recombination along the band gap transition related to the anatase structure of TiO_2 [24, 25]. The band in the range of 400-425 nm is attributed to the emission from the inter-band recombination process of TiO_2 and to self-trapped excitons (STE) [26, 27]. The observed peak at 845 nm is due to the phonon-replica effect [28], where photogenerated electrons and holes recombine by simultaneous emission of phonons and photons. The excited electrons first release one or more phonons to decay to a lower energy level, and from there it emits a photon to decay to the valence band and recombine with a hole.

In Pl measurements, the band gap excitation provides information about the trap sites present in the band gap of TiO_2. The emission peaks at 420, 440, 460, 486, 525 and 548 nm were observed in PL spectra after band gap excitation (385 nm) (**Fig. 8 (a-b))**. Generally, the PL spectra of anatase TiO_2 materials have been attributed to three kinds of physical origins: self-trapped excitons, oxygen vacancies, and the surface state. Peak at 420 and 440 nm is attributed to self-trapped excitons located on the TiO_6 octahedral [27, 29]. PL bands at longer wavelengths in anatase TiO_2 have been attributed to the shallow traps and deep trap emission acting as the radiative centres observed at 460 & 486 nm and 525 & 548 nm respectively [27, 29]. The decrease in intensity of all the above listed peaks for doped TiO_2 is indication of decrease in radiative recombination process along the band gap and within the band gap. In both set of samples (xV4N and 2VxN) the maximum decrease in the intensities of peaks is obtained for 2V4N suggesting minimum recombination process is occurring for this sample. For single V-doped TiO_2 (2V0N)

the peak intensity decreases marginally but as N is introduced with V considerable decrease is visualized. This shows that the codoping of V with N is very effective for charge separation by reducing recombination process which continues to decrease with increasing N concentration even for maximum level of N doping. On the other hand, as V concentration increases above 2V in xV4N sample, the PL intensity again increases to higher values. This indicates that the higher V doping introduces the recombination centres in the form of deep traps of oxygen vacancies within the band gap.

Charge carriers lifetime plays an important role in photocatalytic reactions. The longer charge carrier lifetime lasts, the more photo-generated electrons and holes participate in photocatalytic reactions. To obtain information on the dynamics of photogenerated species under conditions similar to those adopted in our photocatalytic test reactions, time-resolved PL experiment was performed at room temperature and under atmospheric conditions. **Fig. 9** shows the photogenerated electron decay kinetics probed by TRPL with excitation at 405 nm for all the prepared samples. The tri-exponential decay fitting was carried out for the PL signal decay in all investigated materials and led to the decay parameters reported in **Table S1**.The results reveal that the photogenerated carriers in pure TiO_2 recombine much faster than those in the doped and codoped samples. Similar trend is followed in average life time values as that of PL intensity. For single vanadium doped (2V0N; 2.69 ns) and nitrogen doped (0V4N; 3.03 ns) the average life time value increases as compared to pure TiO_2 (1.07 ns). Further increment is observed by introducing both the elements (V & N) in TiO_2 where the values increase with N concentration in 2VxN sample while for xV4N the highest value is recorded for 2V4N. Above this level of V-doping, the average life time decreases.

Both PL and TRPL results suggest that there is reduction in amount as well as delaying in the recombination process. In N-doped TiO_2, the N 2p level formed above the VBM is mainly responsible for trapping photo-generated holes to delay the recombination process. On the other hand, the V 3d states formed below CBM act as the trapping site for electron creating appropriate condition for charge separation. When both these elements are combined in VN-codoped TiO_2 the synergetic effect is established by momentarily trapping both photo-generated electron and holes at impurity levels created by V and N respectively to enhance the charge separation. For V doping, in addition to V 3d states, the deep traps due to oxygen vacancies are also created which act as the recombination centres [30]. This increases the PL emission intensity while decreasing the average life time value for higher V concentration in xV4N sample. Nevertheless, these oxygen vacancies are compensated by N thus improving the charge separation with increase in N concentration in 2VxN-codoped TiO_2 photocatalyst. This shows that N is more effective in reducing the radiative recombination as well as prolonging the lifetime of the charge carrier then V in the codoped TiO_2.

The influence of V and N codoping on intrinsic TiO_2 photocatalytic activity was studied using degradation of PNP and MB as a model reaction under imitated solar light irradiation. The percentage degradation of PNP recorded during light irradiation at specific time intervals is shown in **Fig. 10**. As a reference, the photocatalytic activities of all the prepared samples for MB dye were also carried out as shown in **Fig. S2**. Control experiment shows that PNP and MB is degraded marginally under light in the absence of catalysts for 3 h. Curve of relative concentrations of pollutant were fitted by the first order rate kinetics equation [17] and rate constant is shows in **Table 2**. All the doped and codoped TiO_2 showed higher photocatalytic activity as compared to pure TiO_2. For 2V4N sample, the degradation rate of PNP and MB was 3.04 and 3.07 times higher respectively than the undoped TiO_2. From **Fig. 10**, it can also be seen that the photocatalytic

activity increases as N concentration increases in 2VxN samples, while for V dopant the activity shows an optimum at 2 at% for xV4N TiO_2 samples.

Surface area and particle size, visible light absorption, and recombination process of charges are the main factors affecting the photocatalytic activity. No major variation in either the surface area or particle size is observed upon doping and codoping for both xV4N and 2VxN samples with increase in V or N concentration respectively. The correlation between photocatalytic activity with respect to average life time and band gap for xV4N and 2VxN TiO_2 samples is presented in **Fig. 11**. Both decrease in band gap and increase in average life time value collectively work in enhancing the photocatalytic activity, though the later is more responsible for setting the trend of the curve. Decrease in band gap increases the reaction rate by generating large number of electron-hole pairs by absorption of visible light. These charge pairs require time to travel to the surface to carry out degradation reaction before they recombine. The results clearly demonstrate that in VN-codoped TiO_2 the energy levels formed by V 3d and N 2p states assist in narrowing the band gap and, at the same time, these shallow levels act as the e^- and h^+ trapping sites to prolong the life time of charge carrier. Combination of these phenomenon helps in improving the photocatlytic activity for codoped TiO_2 in comparison to undoped TiO_2. As suggested by absorption and XPS spectra the distinct role of V seems to be decreasing the band gap. Thus as the concentration of V increases leading to the increase in degradation rate upto 2 at. % in xV4N-codoped TiO_2 samples. Above this optimum value the oxygen vacancies are created which forms deep level within the band gap to act as the recombination centres (shown by PL and TRPL) to reduce the activity for higher V doping. The specific role of N is not to majorly affect the band gap but, instead, to act as trapping site for hole and scavenges oxygen vacancy to nullify the deep recombination level for improvement of charge separation. Thus, in short, V improves the visible

light absorption to generate large number of electron-hole pair while N reduces the recombination of electron-hole pair to create the synergetic effect by producing three times better performance than pure TiO_2.

4. Conclusion

This work contributes to a deeper understanding of the specific role of both V and N dopant in VN-codoped TiO_2 during the photocatalytic reaction process. Photoactivity is enhanced by band engineering of TiO_2 by co-doping with vanadium and nitrogen. Nanoparticle size along with large BET surface area of all samples indicates high surface to volume ratio. The surface area is not affected significantly by the presence of the dopant; indeed there is not much variation in particle sizes after doping or codoping in TiO_2. For VN-codoped TiO_2, both dopants give rise to increase in light absorption but vanadium is more effective in narrowing the band gap in VN-codoped TiO_2.Vanadium and nitrogen doping enhance the life time of charge carriers due to the increase in number of trapping centres. Vanadium also creates oxygen vacancy to act as recombination centre but partially filled by nitrogen dopant to reduce the amount of recombination thus improving the lifetime of charge carriers. With regard to the synthesis and characterization of codoped TiO_2 systems, these findings underline the importance to consider dopant induced charge-carrier trapping and recombination effects in the evaluation of the photocatalyst response in order to reach a realistic evaluation of its properties.

Acknowledgements

This work was supported by the Department of Science and Technology, New Delhi (India) in the form of a Women Scientists-A (WOS-A) scheme (Sanction no. SR/WOS-A/PS-62/2012) sanctioned to R. S. Varma. S. Gupta acknowledges DST for providing financial support through National Post-doctoral Fellowship (PDF/2016/004110). We want to acknowledge Sophisticated Analytical Instrument Facility (SAIF) and Central Surface Analytical Facility of IIT Bombay for providing TEM/EDS and XPS facility respectively. N. Patel acknowledge UGC and SERB-DST for providing financial support through Faculty recharge program and Extra Mural project (FILE NO. EMR/2016/003028).

References:

[1] M. Anpo, P. V. Kamat, (eds.), Environmentally Benign Photocatalysts: Applications of Titanium Oxide-based Material, Springer 2010.

[2] S. Lacombe, T. Pigot, Catal. Sci. Technol.**,** 6 **(**2016) 1571-1592.

[3] Mohammad Reza Delsouz Khaki, Mohammad Saleh Shafeeyan, Abdul Aziz Abdul Raman, Wan Mohd Ashri Wan Daud, J. Environ. Manag. 198 (2017) 78-94.

[4] W.Y. Choi, A. Termin, M.R. Hoffmann, J. Phys. Chem-US 84 (1994)13669-13679.

[5] S. Kumar, L. Gomathi Devi, J. Phys. Chem. A 115 (2011) 13211-13241.

[6] R. Jaiswal, N. Patel, D.C. Kothari, A. Miotello, Appl. Catal. B Environ. 126 (2012) 47–54.

[7] Manisha Yadav, Asha Yadav, Rohan Fernandes, Yaksh Popat, Michele Orlandi, Alpa Dashora, D.C. Kothari, Antonio Miotello, B.L. Ahuja, Nainesh Patel, J. Environ. Manag. 203 (2017) 364-374

[8] N. Patel, R. Jaiswal, T. Warang, G. Scarduelli, A. Dashora, B.L. Ahuja, D.C. Kothari, A. Miotello, Appl Catal. B Environ. 150- 151 (2014) 74– 81.

[9] Tamer M. Khedra, Said M. El-Sheikh, Amer Hakki, Adel A. Ismail, Waheed A. Badawy, Detlef W. Bahnemann J Photochem. Photobio. A: Chem. 346 (2017) 530–540

[10] Hayat Khan, Dimitrios Berk, J Photochem. Photobio. A: Chem. 294 (2014) 96–109

[11] R. Jaiswal, J. Bharambe, N. Patel, Alpa Dashora, D.C. Kothari, A. Miotello Appl. Catal B Environ. 168–169, (2015), 333–341.

[12] R. Jaiswal, N. Patel, A. Dashora, R. Fernandes, M. Yadav, R. Edla, R.S. Varma, D.C. Kothari, B.L. Ahuja, A. Miotello, Appl. Catal B: Environ. 183 (2016) 242–253.

[13] S. Livraghi, M. Paganini, E. Giamello, A. Selloni, C.Valentin, and G. Pacchioni, J. Am. Chem. Soc. 128 (2006) 15666-1567.

[14] J. Liu, R. Han, Y. Zhao, H. Wang, W. Lu, T. Yu, Y. Zhang, J. Phys. Chem. C 115(2011) 4507–4515.

[15] D.E. Gu, B.C. Yang, Y.D. Hu, Catal. Commun. 9 (2008) 1472–1476.

[16] N. Makani, K. Tiwari, R. Varma, R. Jaiswal, M. Yadav, D. C. Kothari, N. Patel, I. J. Chem. Phy. Sci. 5 (2015) 59.

[17] R. S. Varma, N.Thorat, R. Fernandes, D. C. Kothari, N. Patel and A. Miotello, Catal. Sci. Technol. 6 (2016) 8428-8440

[18] Y. Wu, H. Liu, J. Zhang, F. Chen, J. Phys. Chem. C 113 (2009) 14689–14695.

[19] G. Yang, Z. Jiang, H. Shi, T. Xiao and Z. Yan, J. Mater. Chem. 20 (2010) 5301–5309.

[20] J. Xu, W. Dai, J. Li, Y. Cao, H. Li, H.He, K. Fan, Catal. Comm. 9 (2008) 146-152.

[21] S. Martha, D. P. Das, N. Biswal, K. M. Parida, J. Mater. Chem. 22 (2012) 10695.

[22] P.Reckers, M.Dimamay, J. Klett, S. Trost,K. Zilberberg, T.Riedl, B. A. Parkinson, J. Brotz, W. Jaegermann, T. Mayer, J. Phys. Chem. C 119 (2015) 9890-9898.

[23] N. Q. Le, I. V. Schweigert, J. Phys. Chem. C 121 (2017) 14254-14260.

[24] B. Liu, L. Wen, X. Zhao, Mater. Chem. Phys. 106 (2007) 350-353.

[25] M. Scepanovic, Z. D. Dohcevic-Mitrovic, I. Hinic, M. Grujic-Brojcin, G. Stanisic, Z. V. Popovic, Mater. Sci. Forum 494 (2005) 265-270.

[26] B. Santara, P. K. Giri, K. Imakita, M. Fujii; Nanoscale5 (2013) 5476-5488.

[27] H. Zhang, M. Zhou, Q. Fu, B. Lei, W. Lin, H. Guo, M. Wu, Y. Lei; Nanotechnology 25 (2014) 275603 (1-10).

[28] M. Gurulakshmi, M. Selvaraj, A. Selvamani, P. Vijayan, N. R. SasiRekha, K. Shanthi, Appl. Catal. A Gen. 449 (2012) 31-46.

[29] F. Montoncello, M. C. Carotta, B. Cavicchi, M. Ferroni, A. Giberti, V. Guidi, C. Malagu, G.Martinelli, F. Meinardi, J. Appl. Phys. 94 (3) (2003) 1501-1505.

[30] B. Choudhury, M. Dey, A. Choudhury, Appl. Nano Sci. 4 (2014) 499-506.

Figure Captions:

Figure 1: XRD patterns of (a) 2VxN and (b) xV4N TiO_2 samples (where x= 0, 1,2,3,4).

Figure 2: XPS spectra in Ti 2p level for (a) pure TiO_2 (b) 2V0N (c) 2V4N and (d) 4V4N TiO_2 samples and in (e) V 2p and (f) N 1s level of 2V4N TiO2 sample.

Figure 3: FTIR spectra of (a) 2VxN and (b) xV4N TiO_2 samples (where x= 0, 1, 2, 3, 4).

Figure 4: UV-Vis absorption spectra of (a) 2VxN (b) xV4N TiO_2 samples (where x= 0, 1,2,3,4).

Figure 5: (a) TEM (b) HRTEM image of 2V4N codoped TiO_2.

Figure 6: EDAX spectra and Elemental mapping of 2V4N codoped TiO_2 powder obtained by TEM/EDS analysis.

Figure 7: PL spectra of (a) 2VxN and (b) xV4N TiO_2 samples (where x= 0, 1, 2, 3, 4) at excitation wavelength of 280 nm.

Figure 8: PL spectra of (a) xV4N and (b) 2VxN TiO_2 samples (where x= 0, 1, 2, 3, 4) at excitation wavelength of 385 nm.

Figure 9: TRPL spectra of (a) 2VxN and (b) xV4N TiO_2 samples (where x= 0, 1, 2, 3, 4) at excitation wavelength of 405 nm.

Figure 10: Photocatalytic degradation of PNP under light irradiation with and without photocatalyst (a) 2VxN (b) xV4N TiO_2 samples (where x= 0, 1, 2, 3, 4)

Figure 11: Correlation of the average lifetime of photo-generated charge carriers and band gap with the photo-degradation rate for the photocatalysts with different dopant concentrations.

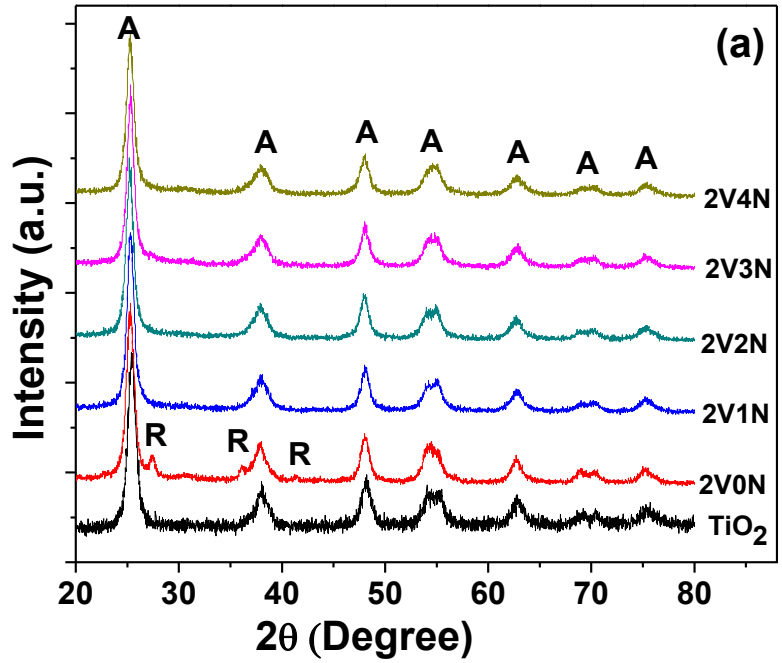
(a)
A
A
A
A
A
A
A
R
R
R
2V4N
2V3N
2V2N
2V1N
2V0N
TiO2
Intensity (a.u.)
20
30
40
50
60
70
80
2θ (Degree)

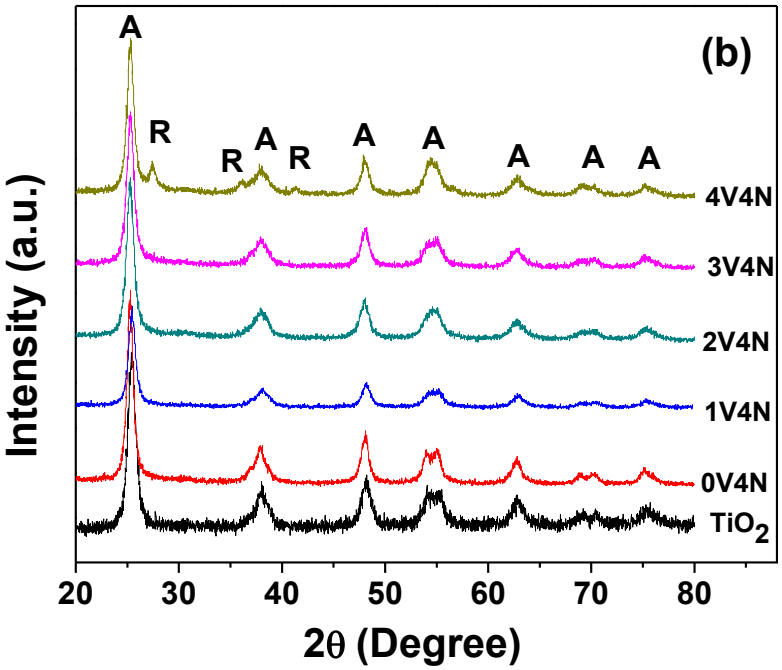
(b)
A
R
R
A
R
A
A
A
A
A
4V4N
3V4N
2V4N
1V4N
0V4N
TiO2
Intensity (a.u.)
20
30
40
50
60
70
80
2θ (Degree)

Figure 1:

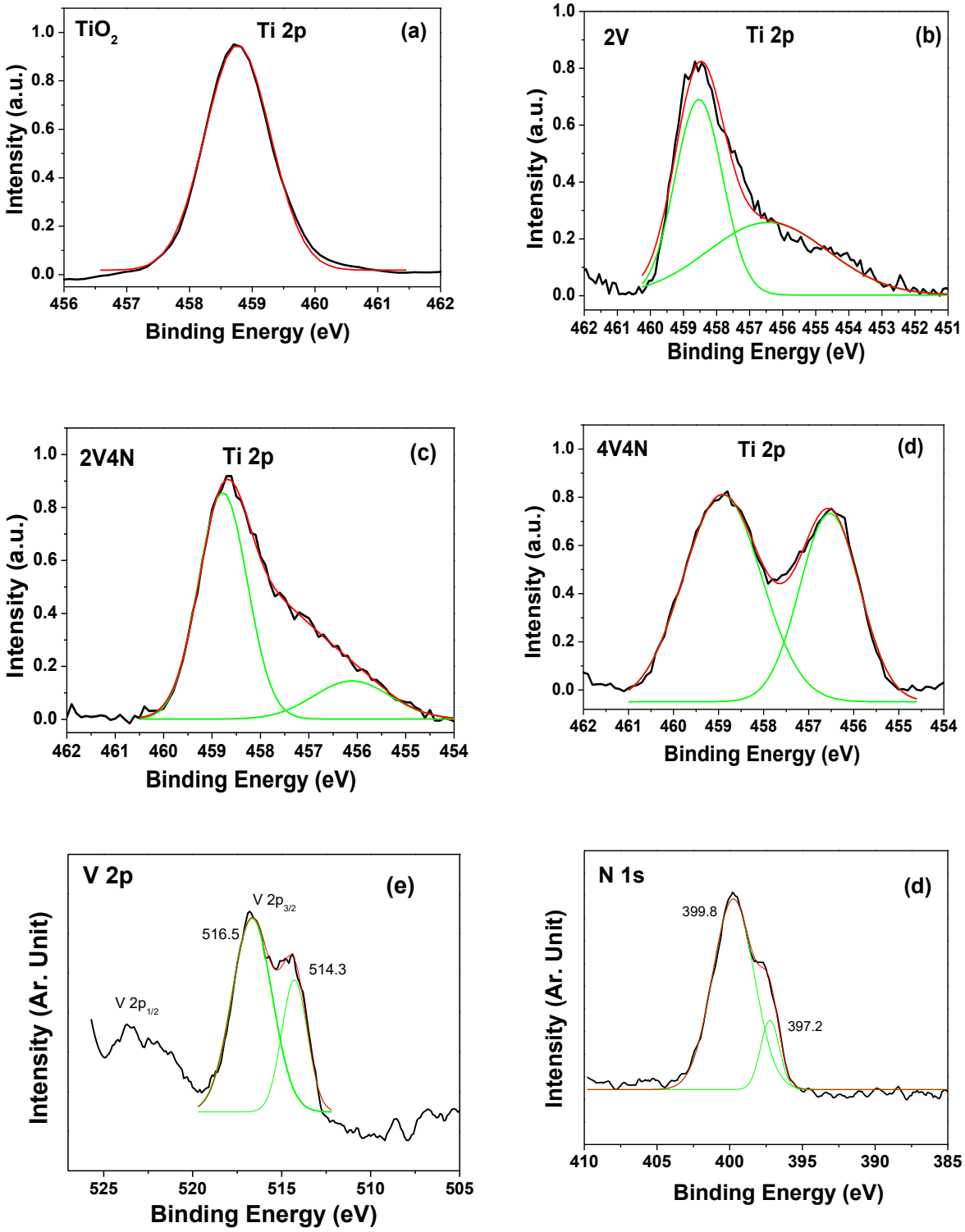
TiO2
Ti 2p
(a)
Intensity (a.u.)
Binding Energy (eV)
2V
Ti 2p
(b)
2V4N
Ti 2p
(c)
4V4N
Ti 2p
(d)
V 2p
(e)
V 2p3/2
V 2p1/2
516.5
514.3
N 1s
(d)
399.8
397.2
Intensity (Ar. Unit)

Figure 2:

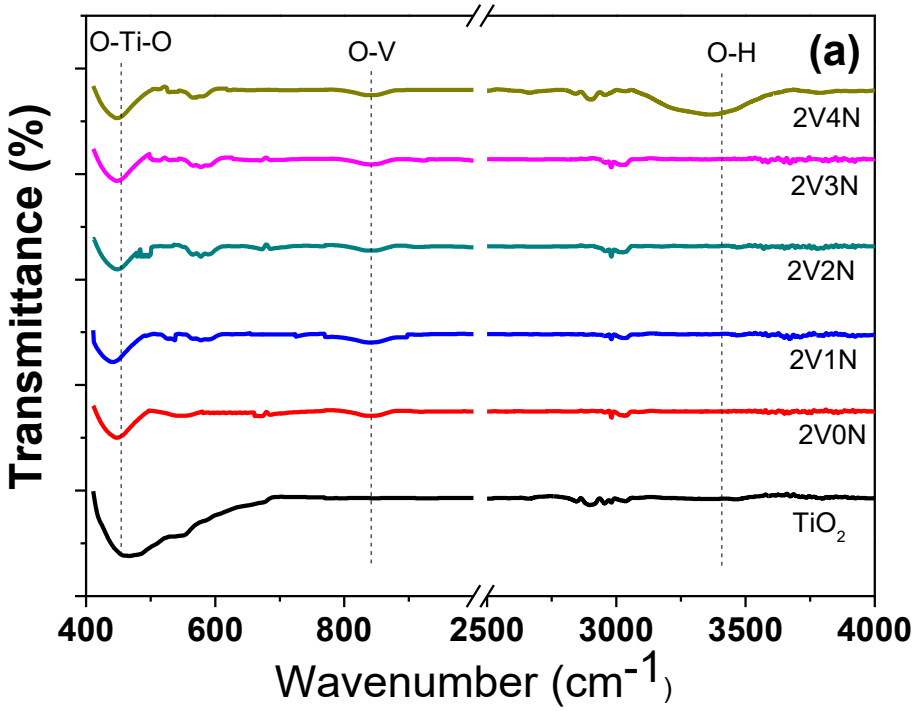
O-Ti-O
O-V
O-H
(a)
2V4N
2V3N
2V2N
2V1N
2V0N
TiO2
Transmittance (%)
400
600
800
2500
3000
3500
4000
Wavenumber (cm-1)

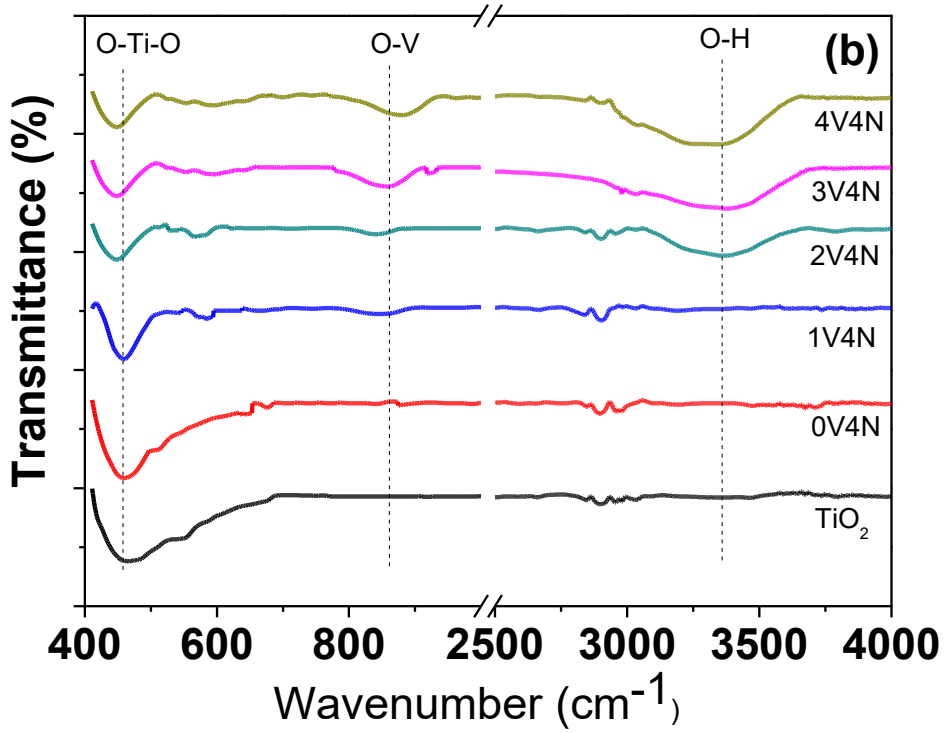
O-Ti-O
O-V
O-H
(b)
4V4N
3V4N
2V4N
1V4N
0V4N
TiO2
Transmittance (%)
400
600
800
2500
3000
3500
4000
Wavenumber (cm-1)

Figure 3:

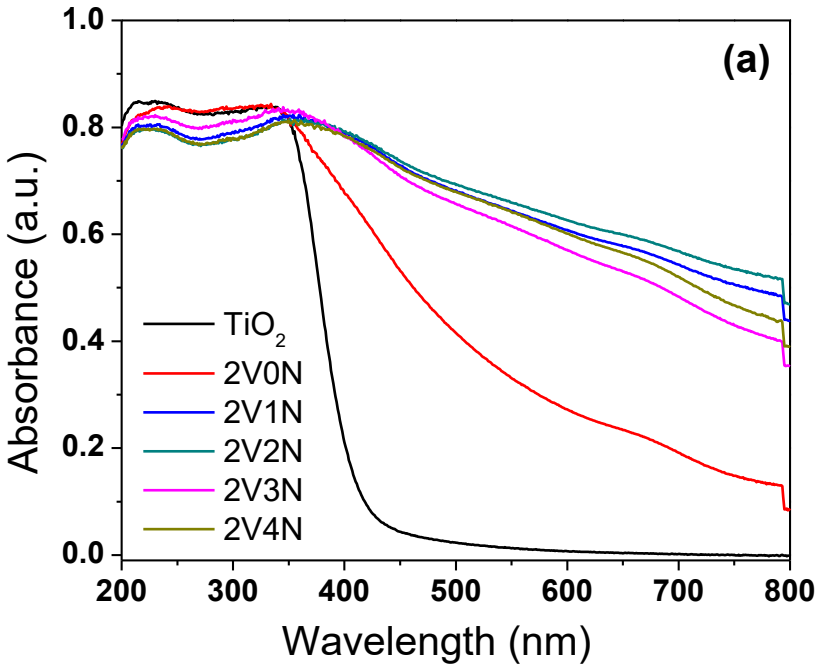
(a)
Absorbance (a.u.)
Wavelength (nm)
TiO2
2V0N
2V1N
2V2N
2V3N
2V4N

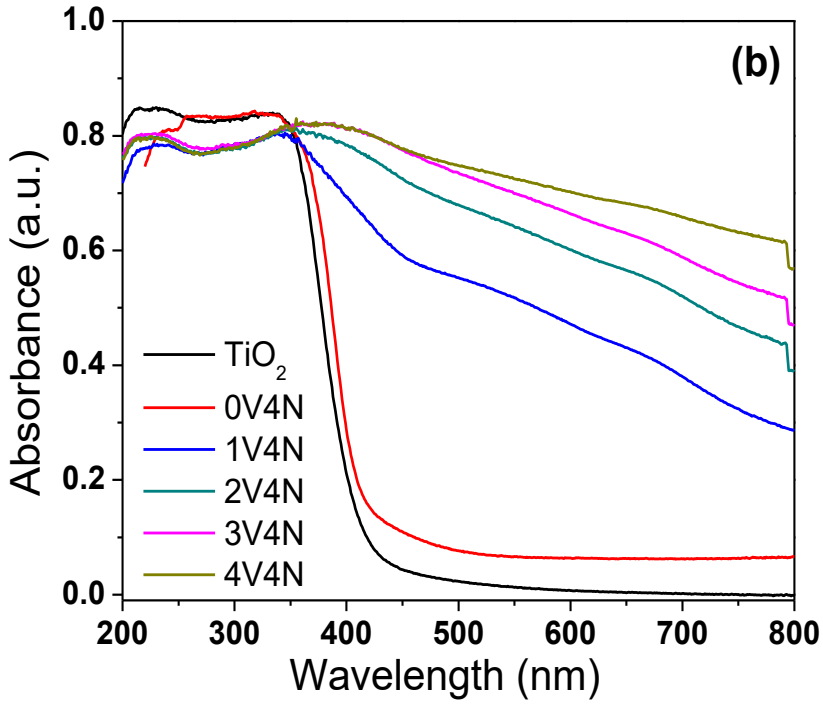
(b)
Absorbance (a.u.)
Wavelength (nm)
TiO2
0V4N
1V4N
2V4N
3V4N
4V4N

Figure 4:

(a)

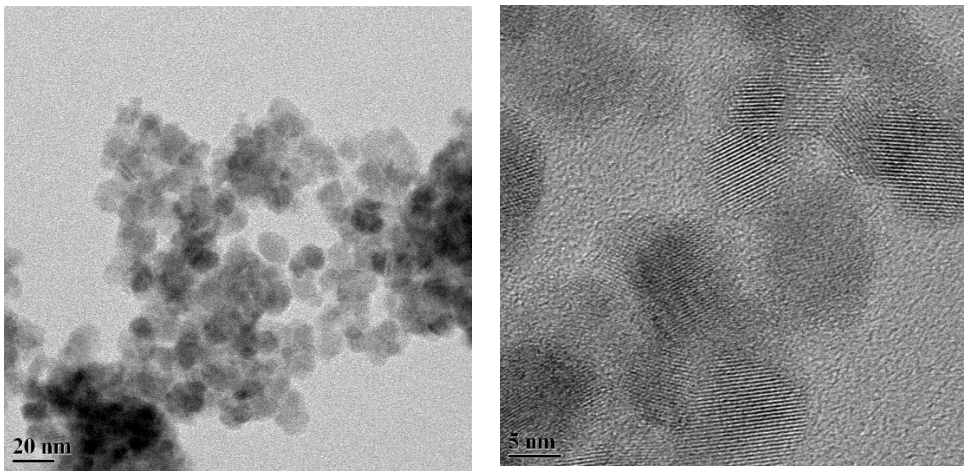

Figure 5:

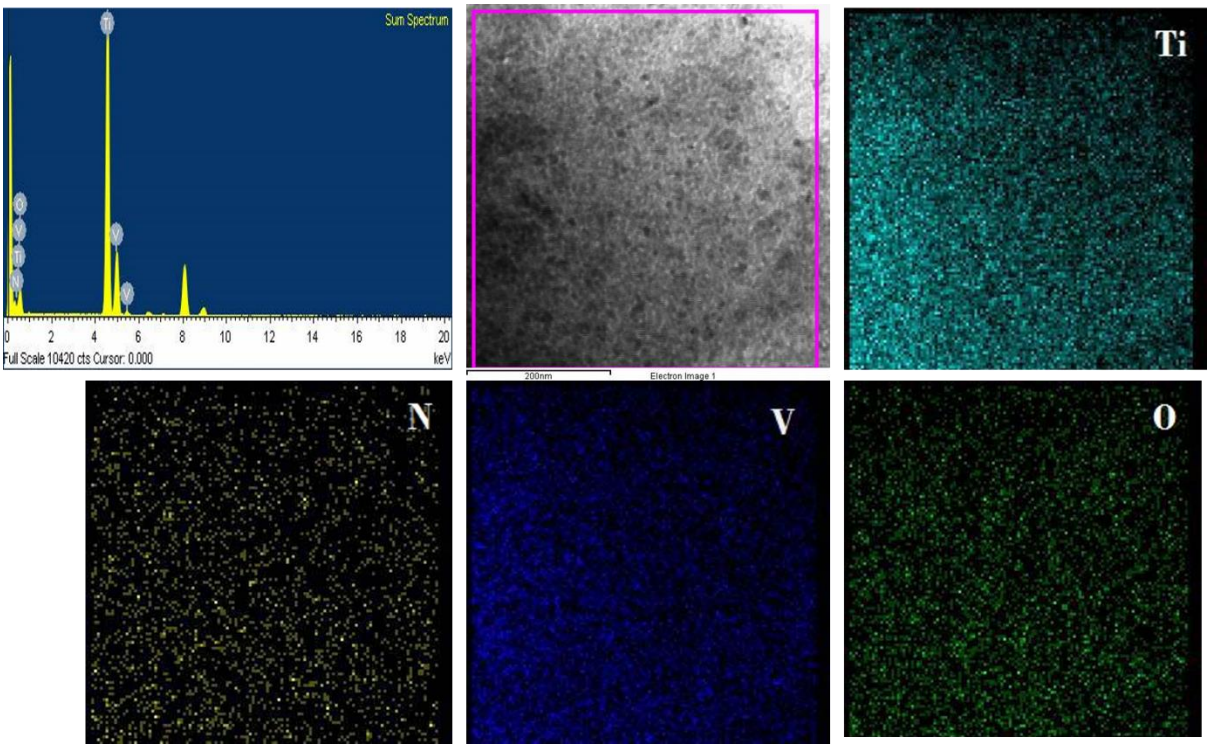
Sum Spectrum
0 2 4 6 8 10 12 14 16 18 20
Full Scale 10420 cts Cursor: 0.000
keV
200nm
Electron Image 1
Ti
N
V
O

Figure 6:

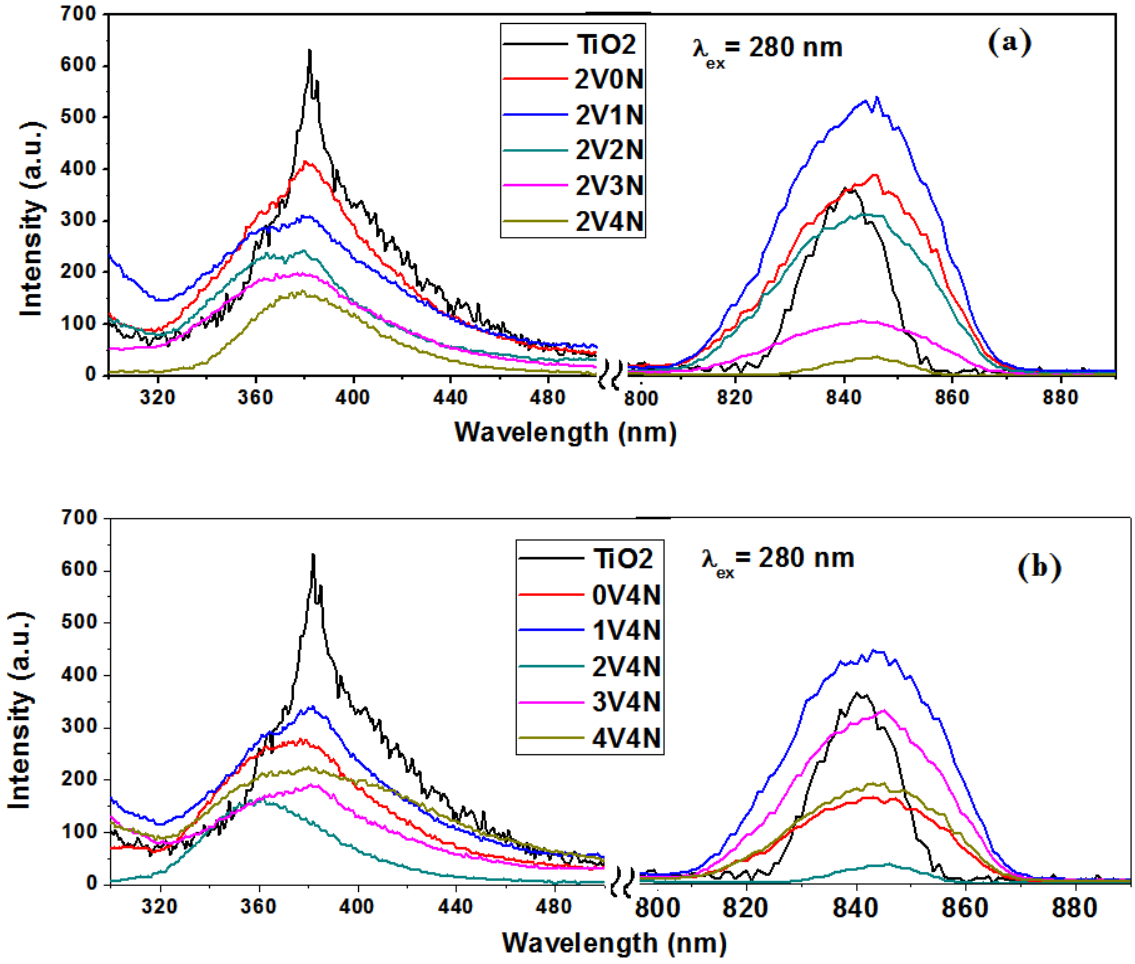
TiO2
2V0N
2V1N
2V2N
2V3N
2V4N
λex = 280 nm
(a)
Intensity (a.u.)
Wavelength (nm)
TiO2
0V4N
1V4N
2V4N
3V4N
4V4N
λex = 280 nm
(b)
Intensity (a.u.)
Wavelength (nm)

Figure 7:

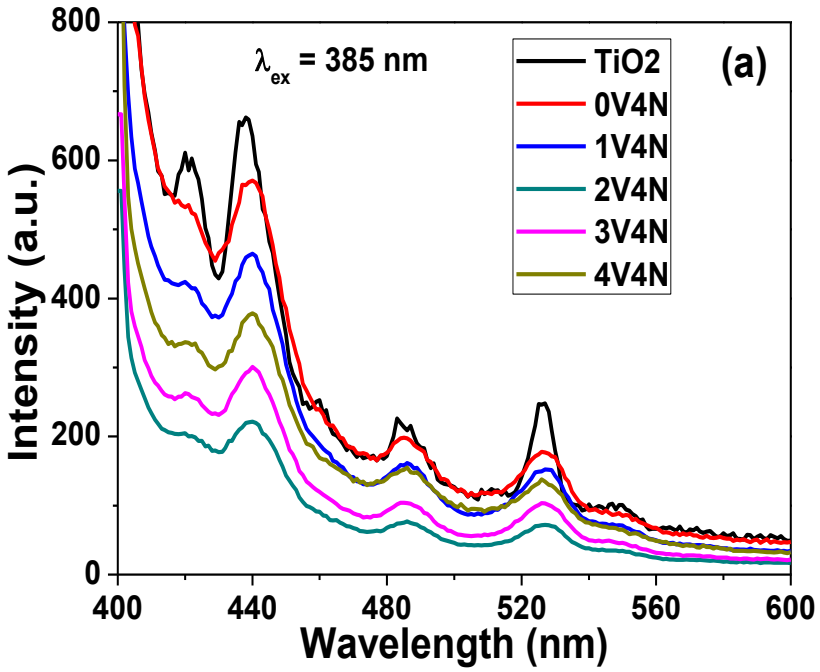
λex = 385 nm
(a)
TiO2
0V4N
1V4N
2V4N
3V4N
4V4N
Intensity (a.u.)
Wavelength (nm)
0
200
400
600
800
400
440
480
520
560
600

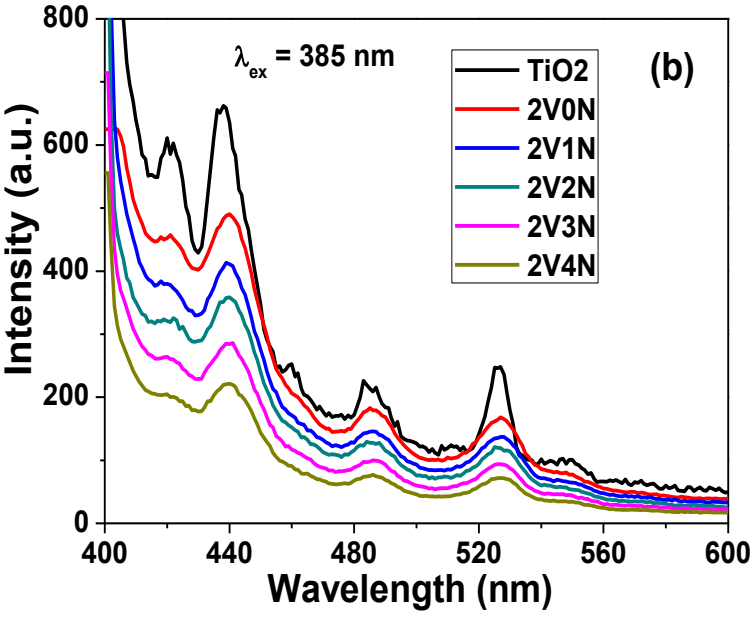
λex = 385 nm
(b)
TiO2
2V0N
2V1N
2V2N
2V3N
2V4N
Intensity (a.u.)
Wavelength (nm)
0
200
400
600
800
400
440
480
520
560
600

Figure 8:

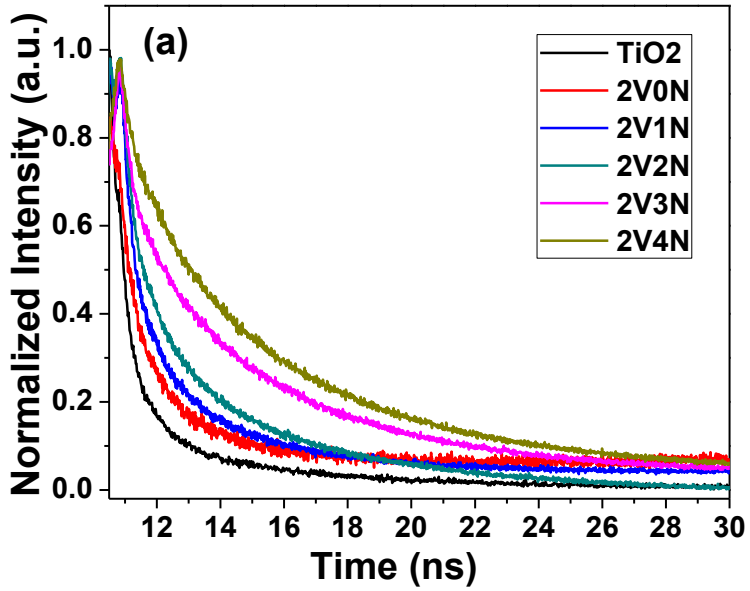
(a)
TiO2
2V0N
2V1N
2V2N
2V3N
2V4N
Normalized Intensity (a.u.)
Time (ns)

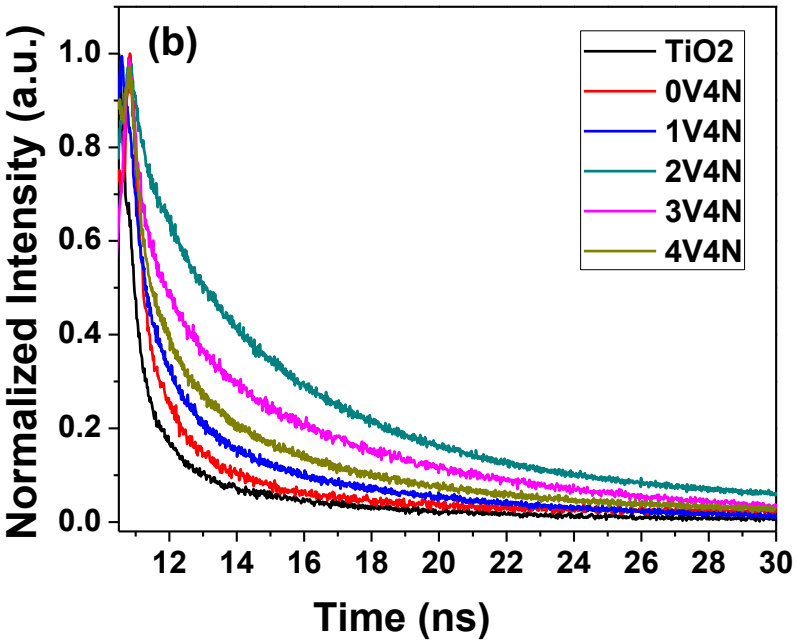
(b)
TiO2
0V4N
1V4N
2V4N
3V4N
4V4N
Normalized Intensity (a.u.)
Time (ns)

Figure 9:

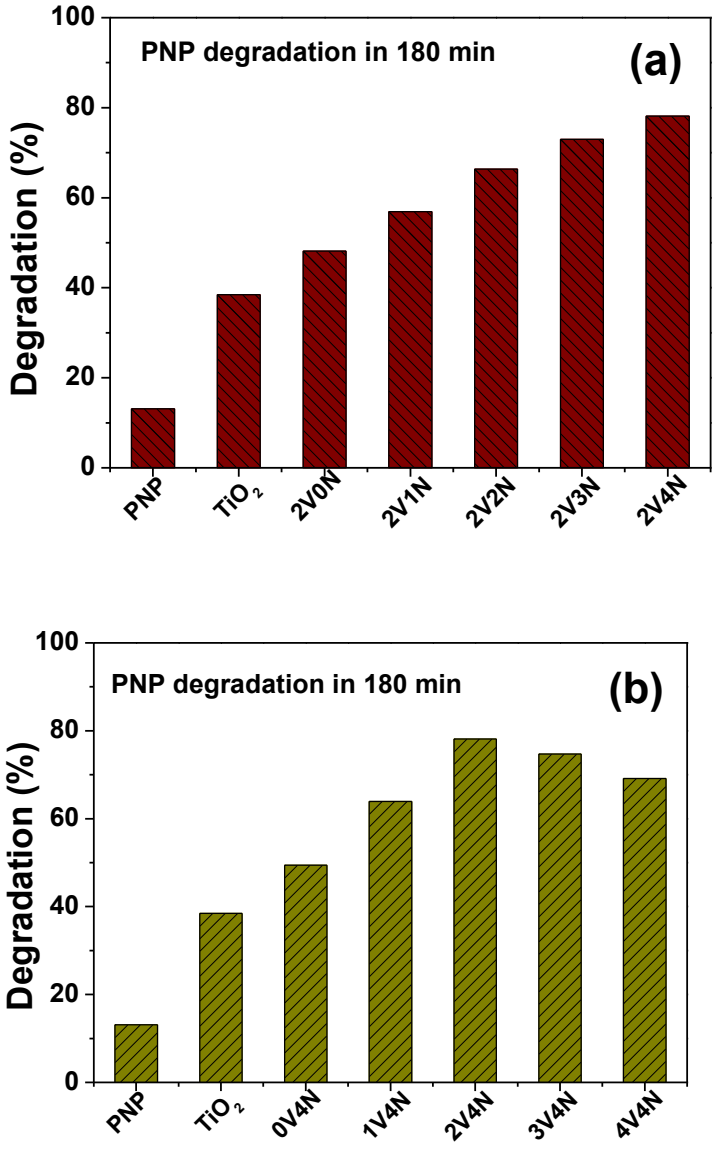
PNP degradation in 180 min
(a)
Degradation (%)
100
80
60
40
20
0
PNP
TiO2
2V0N
2V1N
2V2N
2V3N
2V4N
PNP degradation in 180 min
(b)
Degradation (%)
100
80
60
40
20
0
PNP
TiO2
0V4N
1V4N
2V4N
3V4N
4V4N

Figure 10:

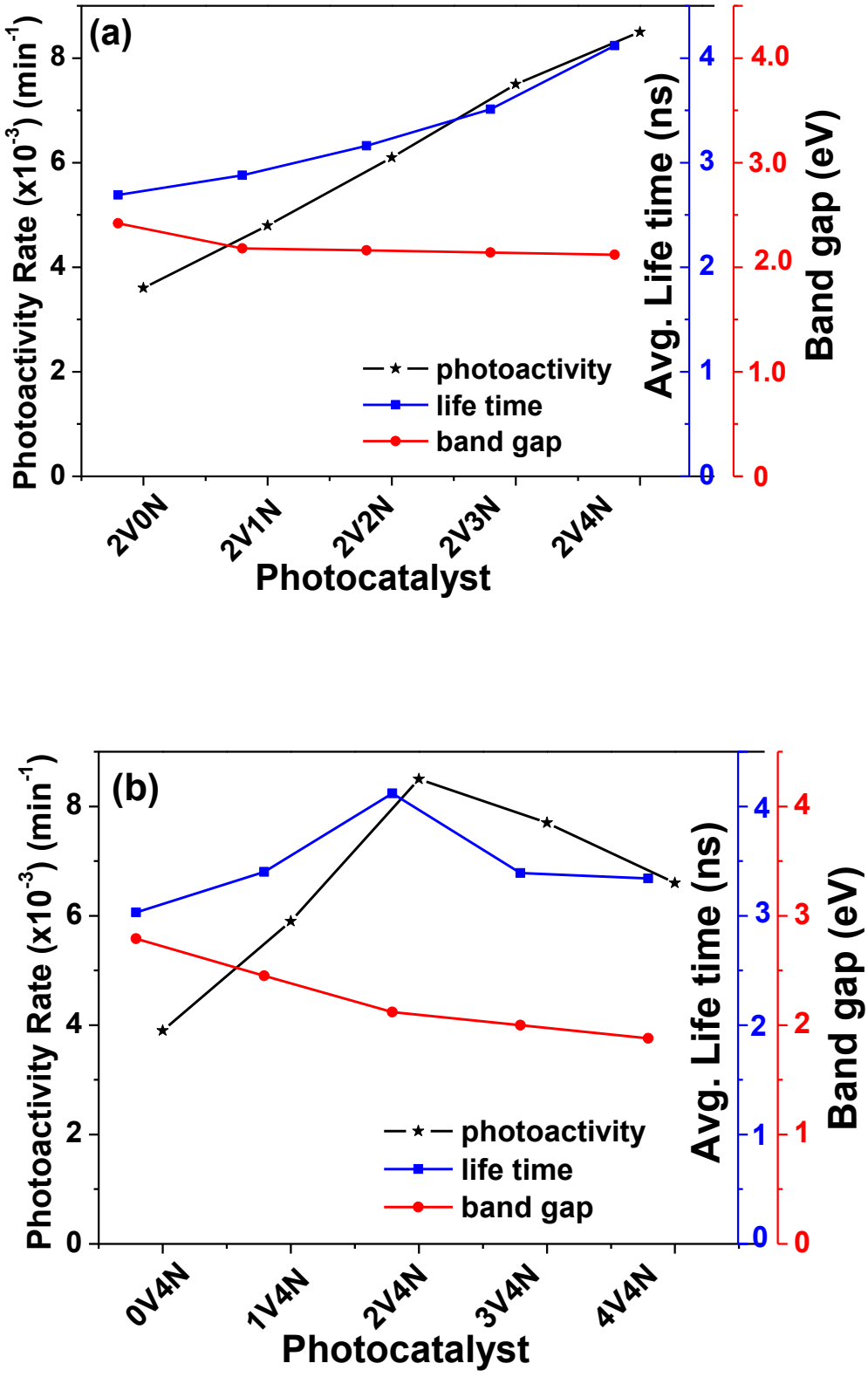
(a)
Photoactivity Rate (x10^{-3}) (min^{-1})
Avg. Life time (ns)
Band gap (eV)
photoactivity
life time
band gap
2V0N
2V1N
2V2N
2V3N
2V4N
Photocatalyst
(b)
Photoactivity Rate (x10^{-3}) (min^{-1})
Avg. Life time (ns)
Band gap (eV)
photoactivity
life time
band gap
0V4N
1V4N
2V4N
3V4N
4V4N
Photocatalyst

Figure 11: